Journal of Materials Chemistry C

PAPER

View Article Online
View Journal | View Issue

Cite this: J. Mater. Chem. C, 2015, 3, 5175

Pure inorganic multi-color electrochromic thin films: vanadium-substituted Dawson type polyoxometalate based electrochromic thin films with tunable colors from transparent to blue and purple†

Lin Liu,[ab] Shi-Ming Wang,*[a] Chao Li,[a] Cheng-Gong Liu,[a] Chun-Lei Ma[a] and Zheng-Bo Han*[b]

Received 24th December 2014,
Accepted 24th March 2015

DOI: 10.1039/c4tc02947j

www.rsc.org/MaterialsC

A polyoxometalate (POM)-based pure inorganic multi-color electrochromic thin film is reported. The films are fabricated by a facile solution-based electrodeposition method. One to three vanadium atoms substituted Dawson type POMs α-$K_{6+n}[P_2W_{18-n}V_nO_{62}]\cdot 18H_2O$ (n = 1, 2, 3) are used as electrochromic materials. With the increase of the amount of vanadium atoms in the molecule, multi-color changes are detected gradually and the performances are also enhanced with the increase of the amount of vanadium atoms. The tri-vanadium substituted POM-based film reveals the highest performance among the three films whose optical contrast is up to 91.8%, and response time for coloration and bleaching is 3.5 s and 3.9 s, respectively. It has a coloration efficiency of 176.8 cm C^{-1} and shows maximum absorption peak shifts at 586 nm, 577 nm and 555 nm followed by the increase of the applied potential. The performances of the films do not show obvious changes after the test of 1000 cycle's consecutive double-potential step chronoamperometric experiments which indicate their good durability.

Introduction

Electrochromic (EC) devices may be electronically darkened or lightened with small applied potentials.[1] The applications of EC devices (ECD) in anti-glare rearview mirrors, safety helmets and displays have also been reported.[2] The widespread use of ECDs depends on the synergistic cooperation of every part of the device. Electrochromic materials are the core part of ECDs, which could be classified into three types: inorganic oxides, organic molecules and polymeric materials.[3] Inorganic oxides feature high thermal stability, the multi-method of processing and high performance of large optical contrast and long durability, and some examples of WO_3 based electrochromic devices have already been applied in the commercial area.[4] EC based-displays could be promising alternatives to liquid crystals or light emission based displays. Tunable colors of ECDs are another important prerequisite for their applications in displays, especially paper-like displays.[5] Compared to organic molecules or polymeric materials, the coloration states of inorganic EC materials are relatively monotonous. In the current state, for mono-component inorganic EC materials, only a single color of different shades was obtained under different applied potentials. That is to say, for mono-component inorganic EC materials different colors could not be obtained by tuning the applied potentials.

There are some strategies for organic molecule or organic polymeric EC materials to obtain multicolor electrochromism, for example, grafting different functional groups to the main organic EC material through molecular tailoring; using different monomers to acquire multicolor organic polymeric EC materials; and so on.[6] Though some of the organic EC materials exhibit fair performance, the crucial issue for the organic EC material based devices is still the stability and durability.[7] And most polymeric EC materials are generally considered to show relatively poor photolytic stability. On the aspects of stability and durability, traditional inorganic EC materials are more competitive with organic EC materials.[8] However, the tuning of extrinsic colors of mono-component inorganic EC materials seemed to be a challenge.[9] Therefore, the exploration of inorganic EC materials or strategies to achieve multicolor changes would be an important step to promote the application of inorganic EC materials to displays.

POMs represent a well-known class of metal oxide nanoclusters with intriguing structures and electrical properties, which have

[a] Light Industry College, Liaoning University, Shenyang 110036, China. E-mail: wangsm383@163.com
[b] College of Chemistry, Liaoning University, Shenyang 110036, China

† Electronic supplementary information (ESI) available. See DOI: 10.1039/c4tc02947j

been applied in many areas such as catalysis, medicine and materials science.[10] The following is a compact introduction of POMs: POMs could be deemed as the polymer of basic metal oxide clusters, such as, $\{WO_3\}$, $\{MoO_3\}$, $\{VO_3\}$, *etc.* Taking tungsten for example, they can form the cluster with the same kind of cluster, for example $[W_{10}O_{32}]^{4-}$, which was classified as isopolyacid; if there was a different atom P or Si in the center of some certain structures of isopolyacid, heteropolyacid was formed, such as, $[XW_{12}O_{40}]^{n-}$ (XW_{12}) or $[X_2W_{18}O_{62}]^{n-}$ (P_2W_{18}), and so on. The aforementioned structural features resulted in the formation of POMs. POMs could also be decorated or designed rationally to obtain certain functions.[11] More importantly, POMs are a class of promising inorganic EC materials. Pioneered by Kurth *et al.*,[12] the research on POM-based EC thin layer-by-layer (LBL) films develop gradually. Like transition metal oxides, their stability is perfect, many can retain their structure up to 500 °C. Moreover, like the organic or polymeric EC materials, the function of the POMs could be tuned through molecular design.[13] Only several groups, for example, Xu group, Ma group and Liu group have devoted their efforts in the investigation of POM based thin EC films using the LBL method.[14] POM based multicolor EC films were also achieved by the combination of POMs and another organic dye or organic EC materials by the LBL method according to the color matching principle.[14i,j] Recently, we have reported a new low cost and facile electrodeposition method to fabricate high performance POM-based EC films. The porous TiO_2 film was used as a substrate for the loading of POMs. The EC films fabricated by the electrodeposition method exhibited excellent performance that featured short response time, high optical contrast and high coloration efficiency.[15] Based on the devisable nature of the POM molecules, the substituted POMs would be an appropriate choice to achieve the real multicolor inorganic EC materials. The substituted POMs whose metal atoms of the basic structure POMs, such as, PW_{12} or X_2W_{18}, could be partly substituted by other transition metals. The transition metal substituted POMs would be helpful to break the single color change of the inorganic EC materials.

In this paper, vanadium substituted Dawson type POMs were chosen as the EC materials. To investigate the effects of vanadium atoms on the colors of EC films, three types of vanadium-substituted POMs, α-$K_{6+n}[P_2W_{18-n}V_nO_{62}]\cdot 18H_2O$ (n = 1, 2, 3), were selected [abb. α-$P_2W_{18-n}V_n$ (n = 1, 2, 3)]. The electrodeposition method was utilized to fabricate the film. The coloration state and the performance of the $P_2W_{18-n}V_n$ (n = 1, 2, 3)-based films were also compared. With the increase of the applied potential, only α-$P_2W_{15}V_3$-based film was observed with obvious color changes from transparent, blue to purple. However, α_2-$P_2W_{17}V$ and α-$P_2W_{16}V_2$-based EC films were detected by SEM and AFM.

Experimental

Materials

α-$K_{6+n}[P_2W_{18-n}V_nO_{62}]\cdot 18H_2O$ (n = 1, 2, 3) were prepared according to literature procedures.[16] The details of the structure of the POMs we used are given in the following paragraphs. The TiO_2 paste with a particle size of *ca.* 18 nm was bought from Dyesol. FTO glass (14 $\Omega\ \square^{-1}$, Nippon Sheet Glass) was purchased from Heptachroma (Dalian, China). The electrolyte is HCl solution (0.1 M). The other reagents were all purchased from Aladdin.

Preparation of the EC electrode

The TiO_2 film with the thickness of *ca.* 6 μm was prepared using the screen printing method. The electrodeposition process is as follows: the counter electrode is a Pt wire; the reference electrode is a SCE and the TiO_2 film acts as a working electrode. The TiO_2 films are immersed in the α-$K_{6+n}[P_2W_{18-n}V_nO_{62}]\cdot 18H_2O$ (n = 1, 2, 3) aqueous solution (1.0 mM); the pH value of the solution was adjusted to ~2 using 1 M HCl. $LiClO_4$ was employed as the supporting electrolyte and the concentration was 0.1 M. Then electrodeposition was carried out using a cyclic voltammogram method between −1.0 and 0.3 V at a scan rate of 100 mV s^{-1} for 30 cycles. After that, the films are rinsed with deionized water and absolute alcohol and then dried in hot air. The film was placed in the oven with the temperature of 150 °C for 30 min.

Film characterization

Electrochemical experiments were performed on a CHI-660D electrochemistry station (Shanghai CH Instrument Corporation, China). The films act as working electrodes; the counter electrode is a Pt wire and the reference electrode is a SCE. Dilute HCl (0.1 M) is used as an electrolyte. Scanning electron microscopy (SEM) was performed using a Hitachi S-4800 scanning electron microscope. Atomic force microscopy (AFM) was performed in air using a SPI3800N Probe Station. Visible light absorption spectra and transmittance spectra were obtained on a Varian Cary 500 UV-vis NIR spectrometer. IR spectra were recorded in the range of 400–2000 cm^{-1} on an Alpha Centaurt FT/IR spectrophotometer on the Si substrate. TG analysis was performed on a Perkin–Elmer TGA7 instrument under air conditions with a heating rate of 10 °C·min^{-1}.

Results and discussion

There are several isomers of the vanadium substituted Dawson type structure.[16] In order to make the different vanadium substituted POMs comparable, the substitution occurring only in the same polar tungsten cluster was used in this paper (Fig. 1). The vanadium substituted POMs still belongs to α-P_2W_{18} with a saturated Dawson structure. For the substitution occurred on the polar site, $P_2W_{17}V$ should be an α_2 isomer. The stability of an EC device is in general determined by two factors: first, the stability of the EC materials; second, the stability of the EC film.[17] Specific to this paper, the stability of the vanadium substituted POMs and the interaction between POMs and the TiO_2 substrate would determine the stability of the films. The stability of the vanadium substituted POMs was tested using thermogravimetric analysis (TGA) under air conditions. As shown in Fig. S1 (ESI†), the V substituted POMs are ultra-stable in the temperature scale of 50 to 600 °C, which enabled the V substituted POMs to be used in a large temperature scale. They also overcome the defects of low stability of the organic

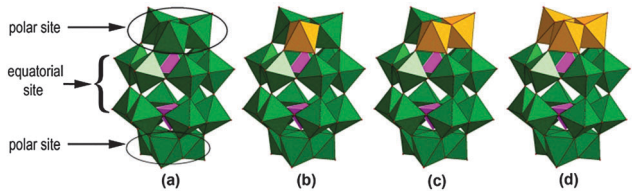

Fig. 1 Structural illustrations of α-P_2W_{18} (a), α_2-$P_2W_{17}V$ (b), α-$P_2W_{16}V_2$ (c) and α-$P_2W_{15}V_3$ (d).

EC materials. The POM-based film was fabricated using an electrodeposition method as we reported before.[15] The cyclic voltammograms measured during preparing thin films are shown in Fig. S2 (ESI†). The peak current density of the cyclic voltammograms increased gradually followed by the increase of the cycles. When approaching 30 cycles, the peak current density almost becomes stable, which indicates that the α-$P_2W_{18-n}V_n$ (n = 1, 2, 3) anions have already reached equilibration when absorbed on TiO_2. 200 cycles of consecutive CV tests were carried out to examine whether the V-POMs could have intense interactions with the TiO_2 substrate. There was no sign of losing the redox current intensity (shown in Fig. S3, ESI†) observed upon performing 200 consecutive CVs. Firstly, hydrogen bonds were formed between oxygen atoms of the α-$[P_2W_{18-n}V_nO_{62}]^{(n+6)-}$ (n = 1–3) POMs and the surface hydroxyl groups (Ti–OH) of the TiO_2 network; secondly, chemically active surface Ti–OH groups were protonated in an acidic medium to form Ti–OH_2^+ groups during the electrodeposition process. The Ti–OH_2^+ group should act as a counter ion for a V substituted Dawson unit and yielded the acid–base reaction. Therefore, it can be concluded that a firm interaction was established between POM molecules and the TiO_2 matrix.[18] The conclusion is also confirmed by the comparison of IR spectra of the composite film, POMs and the TiO_2 substrate. As shown in Fig. 2, the P–O asymmetric stretching vibration of α_2-$P_2W_{17}V$ at 1090 cm^{-1} (Fig. 2b) is split into 3 peaks (1145, 1114 and 1086 cm^{-1} as shown in Fig. 2c) in the composite film. The asymmetric stretching vibrations of W–O–W and W–O–V at 1018, 954 and 920 cm^{-1} are also retained in the films with some shifts (Fig. 2c). Similar results were also detected in the α-$P_2W_{16}V_2$ and α-$P_2W_{15}V_3$ based composite films[16] (as shown in Fig. S4 and S5, ESI†).

The surface morphology and the homogeneity of the POM-based EC film were detected by scanning electron microscopy (SEM) and atomic force microscopy (AFM). As shown in Fig. S6 (ESI†), the size of TiO_2 grains of the as-prepared TiO_2 substrate was *circa* 15 nm, and there is no aggregation of the TiO_2 particles in the substrate. After the deposition of α-$[P_2W_{18-n}V_nO_{62}]^{6-}$ (n = 1–3) on the TiO_2 substrate, the porous structure was still retained as shown in Fig. 3. There was no aggregation of POM molecules in the pores of the TiO_2 substrate which is beneficial for the diffusion of the electrolyte in the composite films and resulted in a short response time of coloration and bleaching.[17,19] The AFM images as shown in Fig. 4, Fig. S7 and S8 (ESI†) further demonstrated that there was no aggregation of POM molecules on the surface of the TiO_2 film. The thickness of the films was

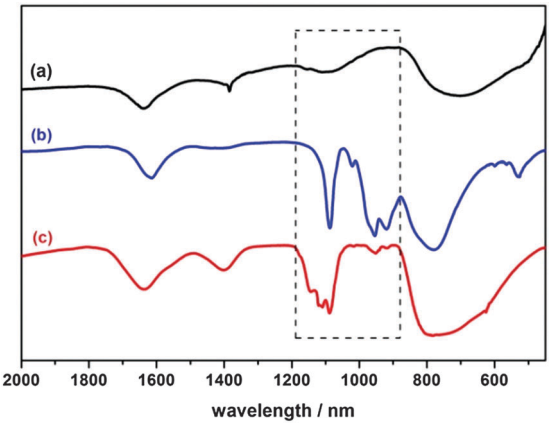

Fig. 2 IR spectra of the TiO_2 substrate (a), α-$K_7[P_2W_{17}VO_{62}]\cdot 18H_2O$ (b) and the composite film (c).

ca. 6 μm after POMs were deposited as determined by a step profiler. The transparency of the films did not change after the deposition of POM molecules (Fig. S9, ESI†).

The diffusion coefficient is an important parameter of the EC film, the cyclic voltammograms (CV) of the EC films at different scan rates in 0.1 M HCl aqueous solution were measured to calculate the diffusion coefficient. As shown in Fig. 5 and Fig. S10 (ESI†), the peak current has a good linear relationship with the square root of the scan rate which indicated that the reaction was fast and is diffusion confined. The diffusion coefficient (D) of H^+ ions has been calculated using Randles–Sevick's equation:[20]

$$D^{1/2} = \frac{I_p/A}{2.72 \times 10^5 \times n^{3/2} \times A \times C_0 \times \upsilon^{1/2}} \quad (1)$$

where I_p is the peak current density, n is the number of electrons, C_0 is the concentration of active ions in the solution, υ is the scan rate, and A is the area of the film. For a film with an area of 0.64 cm^2 and C_0 (H^+) = 0.1 M, the D value of the H^+ ions of the α_2-$P_2W_{17}V$-based EC film was found to be 3.16 × 10^{-11} cm^2 s^{-1}; the D value of the α-$P_2W_{16}V_2$-based EC electrode was 6.98 × 10^{-11} cm^2 s^{-1}; and the D value of the α-$P_2W_{15}V_3$-based EC electrode was 2.44 × 10^{-10} cm^2 s^{-1} Different POM components resulted in different D values.

It exhibited significant differences in the extrinsic hues of the coloration state of the α_2-$P_2W_{17}V$, α-$P_2W_{16}V_2$ and α-$P_2W_{15}V_3$-based EC films. The visible spectra of the $P_2W_{17}V$-based film were recorded under different applied potentials from −1.10 to −1.70 V (Fig. 6a). Under the applied potential of −1.10 V the maximum ABS that occurred at 586 nm is 0.53. With the increase of the applied potential up to −1.70 V, the value of the maximum ABS shows a linear increase up to 0.844 (Fig. 7). The position of the maximum peaks showed a hypsochromic effect from 586 nm to 569 nm (Fig. 8). Though the position of the ABS peak changes, the wavelength scale still belongs to "yellow" and the extrinsic hue of the films did not display obvious changes. For the α-$P_2W_{16}V_2$-based film, the absorption peak is at the wavelength of 590 nm and did not change with increasing applied potential (Fig. S11, ESI†). The coloration of the film exhibited a good linear

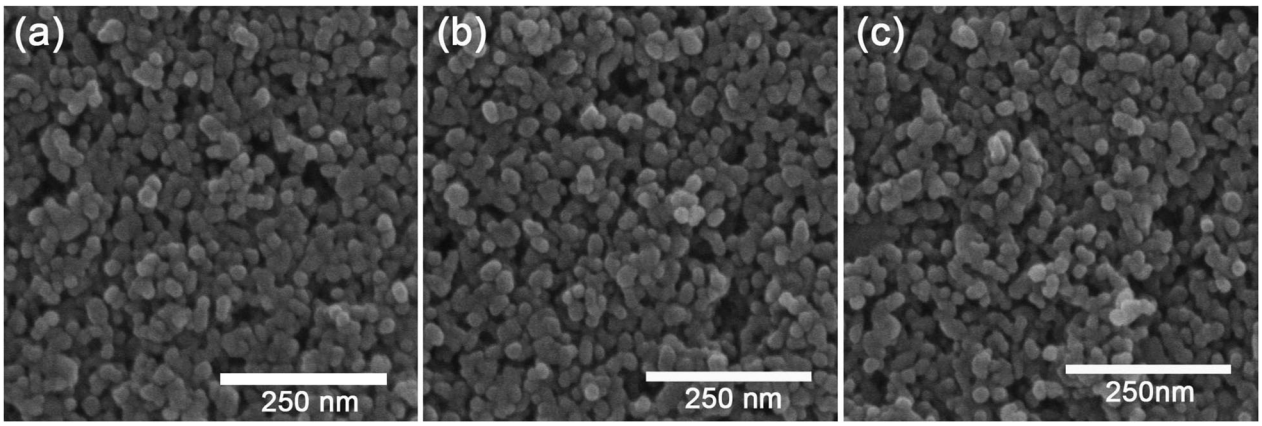

Fig. 3 SEM images of the α_2-$K_7[P_2W_{17}VO_{62}]\cdot 18H_2O$-based composite film (a), α-$K_8[P_2W_{16}V_2O_{62}]\cdot 18H_2O$-based composite film (b) and α-$K_9[P_2W_{15}V_3O_{62}]\cdot 18H_2O$-based composite film (c).

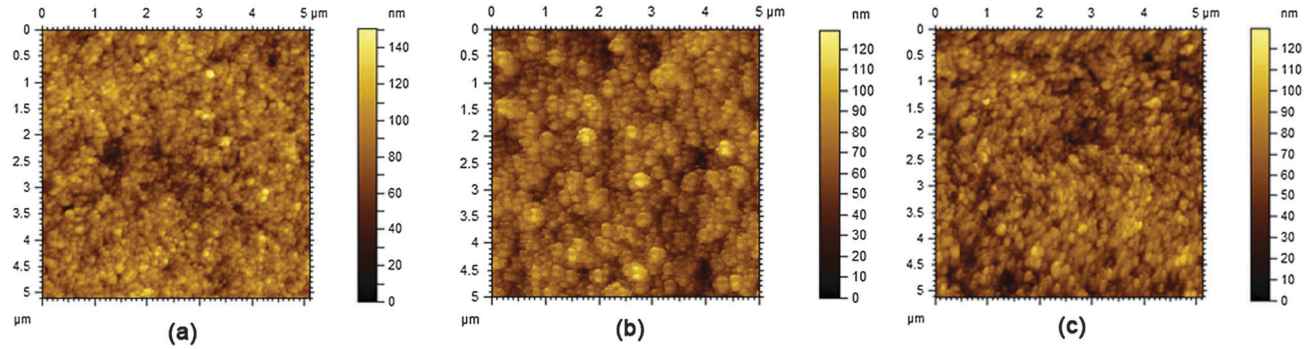

Fig. 4 AFM results of the α_2-$K_7[P_2W_{17}VO_{62}]\cdot 18H_2O$-based composite film (a), α-$K_8[P_2W_{16}V_2O_{62}]\cdot 18H_2O$-based composite film (b) and α-$K_9[P_2W_{15}V_3O_{62}]\cdot 18H_2O$-based composite film (c).

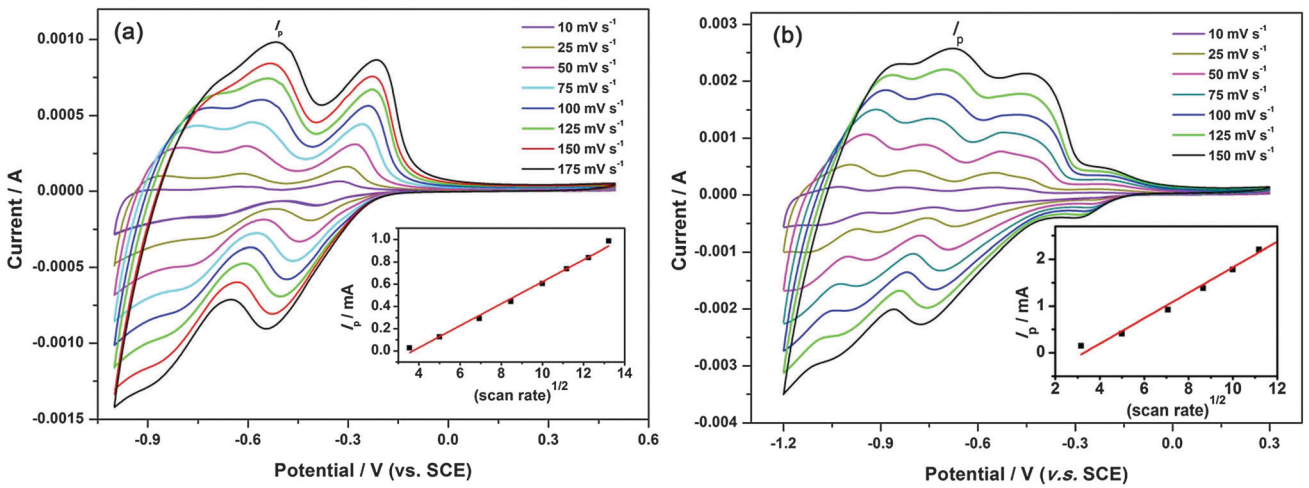

Fig. 5 Cyclic voltammograms (CVs) at different scan rates (10, 25, 50, 75, 100, 125 and 175 mV s^{-1}) of the α_2-$P_2W_{17}V$-based EC film (a) and the α-$P_2W_{15}V_3$-based EC film (b) in HCl (0.1 M) solution. Inset: plots of peak current *versus* the square root of the scan rate.

relationship with the applied potential in the scale of −1.1 V to −1.6 V. However, the color would not turn deeper when the applied potential exceeded −1.6 V. The multicolor phenomenon was only observed in the α-$P_2W_{15}V_3$-based film (Fig. 6b). Under the applied potential from −0.8 V to −1.3 V, the film showed a blue color. And the extent of the color showed a good linear relationship to the applied potential (Fig. 7). Within this potential region the absorption peak has a shift from 586 to 577 nm. The ABS in this region is orange and the corresponding extrinsic color of the film is blue. When the applied potential

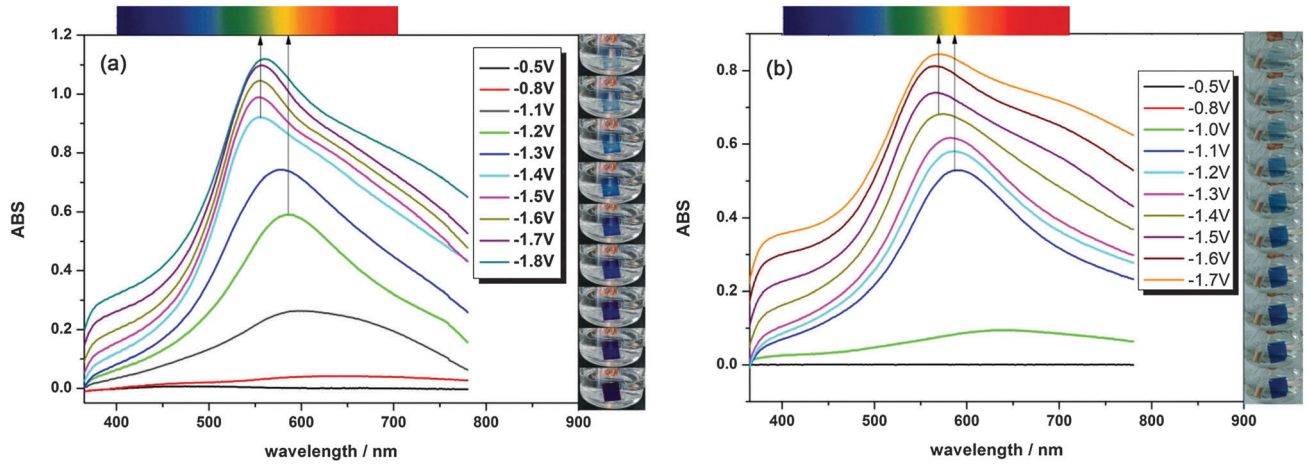

Fig. 6 (a) Visible spectra of the α-$P_2W_{15}V_3$-based EC film recorded under different potentials ranging from −0.5 to −1.8 V. (b) Visible spectra of the α_2-$P_2W_{17}V$-based EC film under different potentials ranging from −0.5 to −1.7 V.

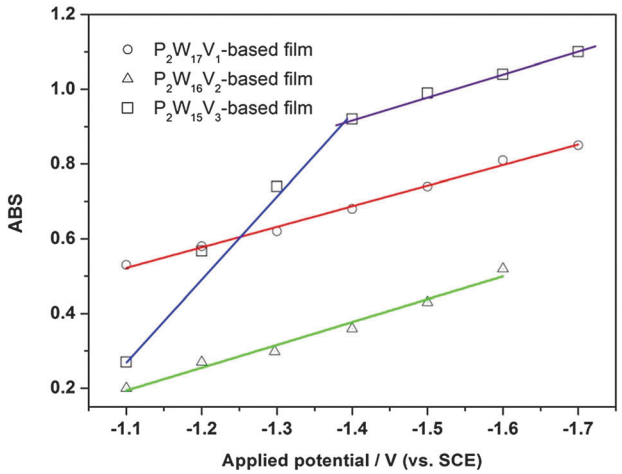

Fig. 7 Comparison of the ABS of three types of EC films under different applied potentials.

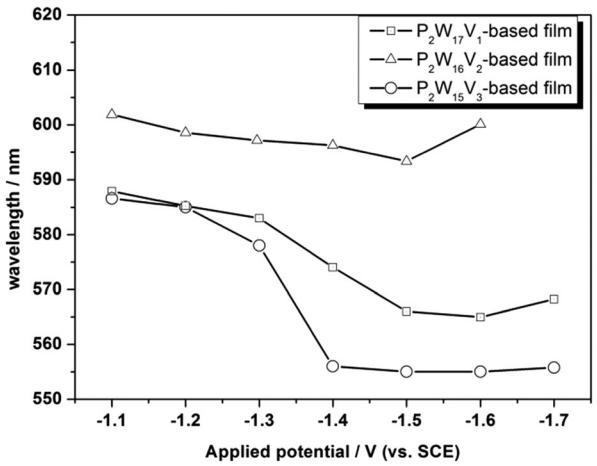

Fig. 8 Maximum ABS wavelength of three types of EC films.

reached −1.4 V, the absorption peak of the film showed a hypsochromic shift to 555 nm. With the increasing potential, the position of the absorption peak is restricted to 555 nm without any shift (Fig. 8). The corresponding extrinsic color of the film is purple. Within the applied potential region of −1.4 to −1.8 V the extent of the color showed a good linear relationship with the applied potentials. Among the three POM based EC films, only the α-$P_2W_{15}V_3$-based EC film showed obvious multi-color changes. This multi-color changes should be attributed to the V substituted W in the Dawson structure. First, the V element has EC activity. With the applied potential increasing, W and V would be colored together which resulted in the extrinsic color of the film turning from blue to purple. According to our previous research, the EC properties of the saturated Daswon type POMs showed relatively low performance. While, the mono-vacant lacunary Dawson structure broke the situation.[15b] According to the literature, the tri-vacant lacunary Dawson structure was unstable when dissolved in water.[21] However, the V atom that occupied the lacunary sites not only stabilized the lacunary structure, but also retained the good EC properties of the lacunary Dawson structure. Second, the number of V atoms is also important. Though the absorption peak of the α_2-$P_2W_{17}V$-based film shows hypsochromic shifts, the amount of V atoms is so small that the multi-color change phenomenon could not be detected with the eye. For the α-$P_2W_{16}V_2$-based film, it showed low performance and nearly no ABS peak change was detected. However, the $P_2W_{15}V_3$-based film revealed totally different results. The performance of the films was nice and the optical contrast almost exceeded the α_2-P_2W_{17}-based EC film at the applied potential of −1.7 V whose optical contrast was the highest among POM-based EC films.[15b] What is more, the multi-color change could be detected with the eye.

To evaluate the performance of the devices, a double-potential step chronoamperometric experiment was conducted by simultaneously recording the transmittance of the device. As shown in Fig. 9a, the double-potential steps were −1.8 to +1.3 V for α-$P_2W_{15}V_3$-based EC films. Fig. 9b and c show the corresponding changes in the current and transmittance. The optical contrast of the α-$P_2W_{15}V_3$-based EC film was 91.8% (λ = 555 nm)

at the applied potential of −1.8 V. A residual leakage current was rapidly achieved during coloration and the current decays rapidly to zero during bleaching for the three EC films. Similar double-potential step chronoamperometric experiments were also performed to test α_2-$P_2W_{17}V$ and α-$P_2W_{16}V_2$-based EC films. The results are recorded in Fig. S12 (ESI†), the optical contrast of the α_2-$P_2W_{17}V$-based EC film was 85.1% (λ = 565 nm) under the double-potential steps of −1.7 to +1.5 V. The optical contrast of the α-$P_2W_{16}V_2$-based EC film was 48.3% (λ = 590 nm) under the double-potential steps of −1.6 to +1.3 V (Fig. S13, ESI†). The bleaching state of the films is transparent and the coloration state of the films exhibits different colors. For the α_2-$P_2W_{17}V$-based film, the coloration state is deep blue; for the α-$P_2W_{16}V_2$-based film, the coloration state is blue; and for the α-$P_2W_{15}V_3$-based film, the coloration state is blue and purple. The stability and reversibility of the α-$P_2W_{18-n}V_n$ (n = 1–3)-based EC films were also tested by repetitive double-potential step chronoamperometric experiments. As shown in Fig. S14 (ESI†), the response time for coloration and bleaching, and the optical contrast of the α-$P_2W_{18-n}V_n$ (n = 1–3)-based EC films did not change noticeably even after 10^3 cycles. It is also found to be stable for more than 10^3 cycles.

As shown in Fig. 10, the coloration/bleaching time extracted for a 90% transmittance change which was an important criterion for judging an EC film is detected to be 3.5 s ($t_{c,90\%}$) and 3.9 s ($t_{b,90\%}$) for the α-$P_2W_{15}V_3$-based EC film. And for the α_2-$P_2W_{17}V$-based EC film, the coloration time is little longer than the α-$P_2W_{15}V_3$-based EC film with $t_{c,90\%}$ = 5.6 s, and the bleaching time $t_{b,90\%}$ = 4.1 s. However, the α-$P_2W_{16}V_2$-based film is more difficult to be colored and its $t_{c,90\%}$ is 11.1 s and $t_{b,90\%}$ is 4.5 s. The coloration efficiency (CE) is also a crucial parameter to judge an EC film which represents the change in the optical contrast (ΔOD) for the charge consumed per unit of electrode area. It can be calculated from the following formula:[22]

$$\mathrm{CE}(\eta) = \frac{\Delta \mathrm{OD}}{q/S} = \frac{\Delta A}{q/S} = \frac{\log(T_b/T_c)}{q/S} \quad (2)$$

where ΔOD is the optical contrast at a given wavelength λ, q is the injected electronic charge, S is the electrode area, ΔA is the absorbance change, T_b and T_c are the transmittances of the

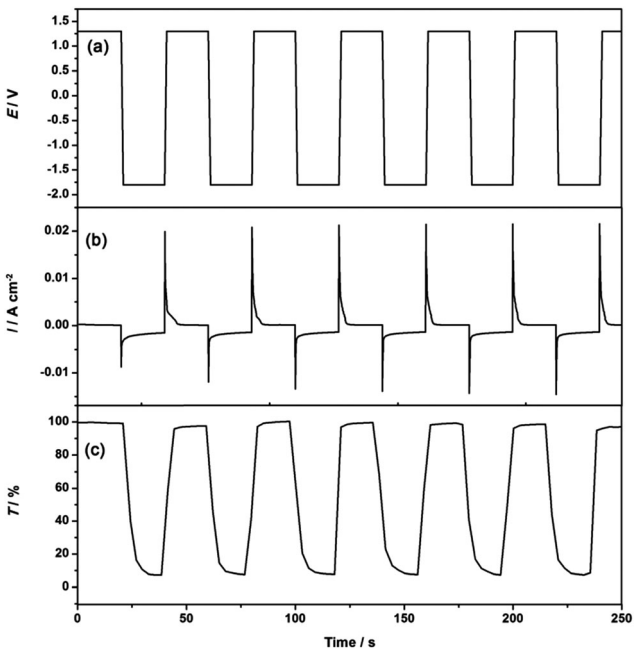

Fig. 9 Potential (a), current (b) and transmittance (c) at 620 nm of the α-$P_2W_{15}V_3$-based EC film during the subsequent double-potential step chronoamperometric experiments of −1.8 V to +1.3 V.

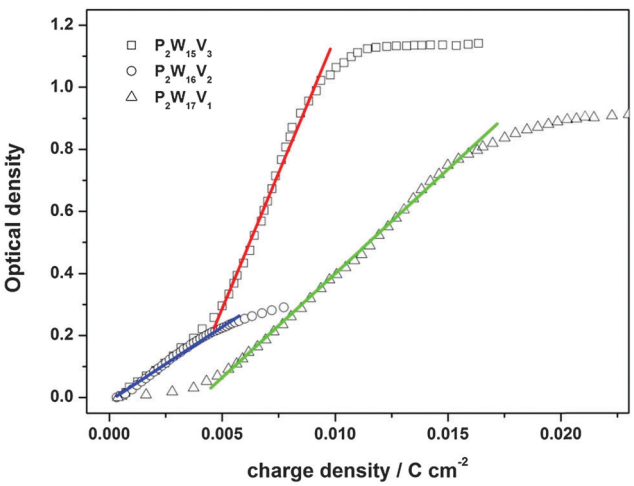

Fig. 11 Plot of optical density *versus* charge density for the α_2-$P_2W_{17}V$-, α-$P_2W_{16}V_2$- and α-$P_2W_{15}V_3$-based EC films.

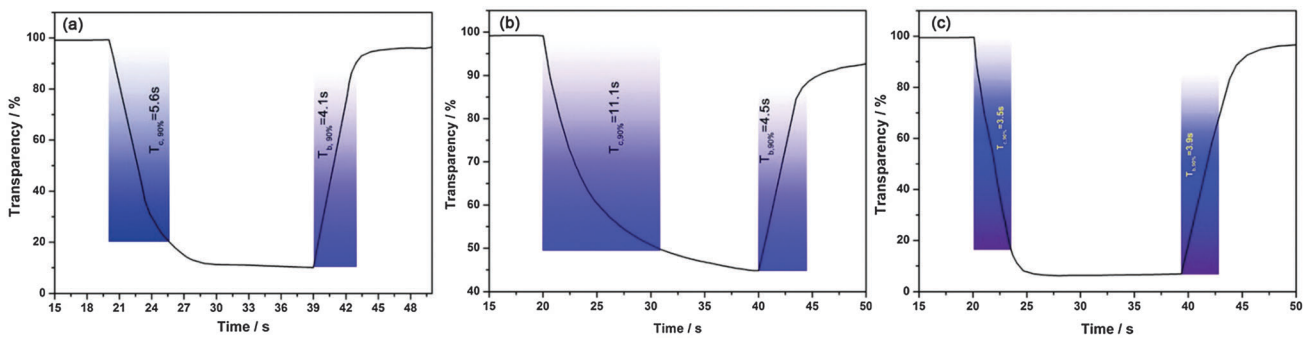

Fig. 10 Coloration/bleaching time extracted for a 90% transmittance change for the (a) α_2-$P_2W_{17}V$-, (b) α-$P_2W_{16}V_2$- and (c) α-$P_2W_{15}V_3$-based EC films.

Table 1 Some parameters of the α_2-$P_2W_{17}V$-, α-$P_2W_{16}V_2$- and α-$P_2W_{15}V_3$-based EC films

EC film	Optical contrast$_{(max)}$	λ_{max}/nm	Color modulation	$t_{c,90\%}/t_{b,90\%}$/s	CE/cm^2 C^{-1}
α_2-$P_2W_{17}V$	85.1% (λ = 565 nm)	586, 569	Transparent → blue	5.6/4.1	67.7
α-$P_2W_{16}V_2$	48.3% (λ = 590 nm)	590	Transparent → blue	11.1/4.5	47.8
α-$P_2W_{15}V_3$	91.8% (λ = 555 nm)	586, 577, 555	Transparent → blue → purple	3.5/3.9	176.8
α-P_2W_{18}[a]	48.7% (λ = 646 nm)	646	Transparent → blue	0.97/1.98	176.8
α_2-P_2W_{17}[a]	93.1% (λ = 620 nm)	620	Transparent → blue	0.90/2.81	205.3

[a] The data are from ref. 15*b*.

bleached and colored states, respectively. The CE is extracted as the slope of the line fits to the linear region of the curve. The comparison of the CE of three types of EC films is illustrated in Fig. 11. The calculated CE values are 67.6, 47.8 and 176.8 cm^2 C^{-1} for α_2-$P_2W_{17}V$, α-$P_2W_{16}V_2$ and α-$P_2W_{15}V_3$-based EC films, respectively. The CE value of the α-$P_2W_{15}V_3$-based EC film is the highest. The higher CE value indicated that the α-$P_2W_{15}V_3$-based EC film exhibited a large optical modulation with a small charge introduced (or extracted). In order to compare the performance of three EC films clearly, the parameters of the V-substituted POM-based EC film were also gathered in Table 1. It could be concluded that the V atoms in the Dawson basic structure not only affected the color modulation region of the EC films, but also affected the electrochemical properties. They all adopt the saturated structure for the three V substituted Dawson molecules. With the increase of the amount of the larger electronegative V^{5+}, it is easier to attract electrons. But the bi-vanadium substituted α-P_2W_{18} is an exception whose performance is the lowest. This might be partly because α-$P_2W_{16}V_2$ could be regarded as the combination of V_2 and P_2W_{16} which is an unstable intermediate with low electroactivity. For α_2-$P_2W_{17}V$ and α-$P_2W_{15}V_3$, the performance was enhanced by increasing the substitution degree. The electron was first attracted by the more electronegative V^{5+} on the polar site of the Dawson anion, then the electrons pass to the W^{6+} anions on the equatorial site which are easier to be reduced than the W^{6+} anions on the polar sites. While, α-$P_2W_{15}V_3$ has three V^{5+} to attract electrons and six vertice-shared W^{6+} anions on the equatorial site, α_2-$P_2W_{17}V$ has only one V^{5+} to attract electrons and two vertice-shared W^{6+} anions on the equatorial site. Obviously, α-$P_2W_{15}V_3$ has more EC active sites compared to α_2-$P_2W_{17}V$. Therefore, the α-$P_2W_{15}V_3$-based film is easier to be reduced, which results in a shorter coloration/bleaching time of 3.5/3.9 s and a higher CE value of 176.8 cm^2 C^{-1}.

Conclusions

In conclusion, multi-color pure inorganic EC films have been prepared successfully for the first time. Color modulation from transparent to blue and purple achieved by using an electrodeposited film of α-$P_2W_{15}V_3$ as EC material and nano-TiO_2 as a substrate. The structures of the V-substituted Dawson POMs (α_2-$P_2W_{17}V$, α-$P_2W_{16}V_2$ and α-$P_2W_{15}V_3$) are nearly the same but only the tri-vanadium substituted structure α-$P_2W_{15}V_3$ showed multi-color modulation. Therefore, adjusting the components of a POM molecule is an effective strategy to find new POM-based inorganic EC materials, especially the multi-color modulation EC materials. The multi-color inorganic POM-based EC films have great potential to be applied in EC displays. This may be an important breakthrough in inorganic EC materials area. The POM-based films with other colors are under investigation.

Acknowledgements

This work was financially supported by the National Natural Science Foundation of China (51102125), the Liaoning Province Doctor Startup Fund (20141052), the Natural Science Foundation of Liaoning (201102081) and the Youth Science Research Foundation of Liaoning University (2013LDQN19 and LDGY201412).

Notes and references

1 (*a*) C. M. Lampert, *Sol. Energy Mater. Sol. Cells*, 2003, **76**, 489; (*b*) M. Green and K. Pita, *Sol. Energy Mater. Sol. Cells*, 1996, **43**, 393; (*c*) D. T. Gillaspie, R. C. Tenent and A. C. Dillon, *J. Mater. Chem.*, 2010, **20**, 9585; (*d*) K. Wang, H. Wu, Y. Meng, Y. Zhang and Z. Wei, *Energy Environ. Sci.*, 2012, **5**, 8384.

2 (*a*) H. J. Byker and J. H. Bechtel, *US. Pat.*, 4,917,477, 1990; (*b*) C. G. Granqvist, *Nat. Mater.*, 2006, **5**, 89; (*c*) T. Kobayashi, H. Yoneyama and H. Tamura, *J. Electroanal. Chem. Interfacial Electrochem.*, 1984, **161**, 419.

3 (*a*) C. G. Granqvist, *Adv. Mater.*, 2003, **15**, 1789; (*b*) J. Zhang, J. P. Tu, X. H. Xia, X. L. Wang and C. D. Gu, *J. Mater. Chem.*, 2011, **21**, 5492; (*c*) W. Lu, A. G. Fadeev, B. Qi, E. Smela, B. R. Mattes, J. Ding, G. M. Spinks, J. Mazurkiewicz, D. Zhou, G. G. Wallace, D. R. MacFarlane, S. A. Forsyth and M. Forsyth, *Science*, 2002, **297**, 983; (*d*) P. M. Beaujuge, S. Ellinger and J. R. Reynolds, *Nat. Mater.*, 2008, **7**, 795.

4 E. S. Lee and D. L. DiBartolomeo, *Sol. Energy Mater. Sol. Cells*, 2002, **71**, 465.

5 (*a*) C. G. Granqvist, *Sol. Energy Mater. Sol. Cells*, 2000, **60**, 201; (*b*) U. Bach, D. Corr, D. Lupo, F. Pichot and M. Ryan, *Adv. Mater.*, 2002, **14**, 845.

6 (*a*) K. Wang, T. Zhang, Y. Hu, W. Yang and Y. Shi, *Electrochim. Acta*, 2014, **130**, 46; (*b*) G. F. Cai, J. P. Tu, D. Zhou, J. H. Zhang, X. L. Wang and C. D. Gu, *Sol. Energy Mater. Sol. Cells*, 2014, **122**, 51; (*c*) Y. W. Chuang, H. J. Yen, J. H. Wu and G. Sh. Liou, *ACS Appl. Mater. Interfaces*, 2014, **6**, 3594; (*d*) J. Sun, X. Lv, P. Wang, Y. Zhang, Y. Dai, Q. Wu, M. Ouyang and C. Zhang, *J. Mater. Chem. C*, 2014, **2**, 5365; (*e*) A. A. Argun, P. H. Aubert, B. C. Thompson, I. Schwendeman,

C. L. Gaupp, J. Hwang, N. J. Pinto, D. B. Tanner, A. G. MacDiarmid and J. R. Reynolds, *Chem. Mater.*, 2004, **16**, 4401; (*f*) Y. Y. Song, Z. D. Gao, J. H. Wang, X. H. Xia and R. Lynch, *Adv. Funct. Mater.*, 2011, **21**, 1941; (*g*) J. Matsui, R. Kikuchi and T. Miyashita, *J. Am. Chem. Soc.*, 2014, **136**, 842.

7 J. Zhang, J. Tu, D. Zhang, Y. Qiao, X. Xia, X. Wang and C. Gu, *J. Mater. Chem.*, 2011, **21**, 17316.

8 (*a*) D. T. Gillaspie, R. C. Tenent and A. C. Dillon, *J. Mater. Chem.*, 2010, **20**, 9585; (*b*) P. R. Somani and S. Radhakrishnan, *Mater. Chem. Phys.*, 2002, **77**, 117.

9 G. Cai, J. Tu, D. Zhou, J. Zhang, Q. Xiong, X. Zhao, X. Wang and C. Gu, *J. Phys. Chem. C*, 2013, **117**, 15967.

10 (*a*) H. Lv, W. Guo, K. Wu, Z. Chen, J. Bacsa, D. G. Musaev, Y. V. Geletii, S. M. Lauinger, T. Lian and C. L. Hill, *J. Am. Chem. Soc.*, 2014, **136**, 14015; (*b*) X. B. Han, Z. M. Zhang, T. Zhang, Y. G. Li, W. Lin, W. You, Z. M. Su and E. B. Wang, *J. Am. Chem. Soc.*, 2014, **136**, 5359; (*c*) Q. Tang, Y. Liu, S. Liu, D. He, J. Miao, X. Wang, G. Yang, Z. Shi and Z. Zheng, *J. Am. Chem. Soc.*, 2014, **136**, 12444; (*d*) J. Borges, L. C. Rodrigues, R. L. Reis and J. F. Mano, *Adv. Funct. Mater.*, 2014, **24**, 5624; (*e*) D. Zhou and B. H. Han, *Adv. Funct. Mater.*, 2010, **20**, 2717; (*f*) C. L. Hill, *Chem. Rev.*, 1998, **98**, 1; (*g*) T. R. Zhang, S. Q. Liu, D. G. Kurth and C. F. J. Faul, *Adv. Funct. Mater.*, 2009, **19**, 642; (*h*) A. Proust, R. Thouvenot and P. Gouzerh, *Chem. Commun.*, 2008, 1837; (*i*) S. M. Wang, L. Liu, W. L. Chen, Z. M. Su, E. B. Wang and C. Li, *Ind. Eng. Chem. Res.*, 2014, **53**, 150; (*j*) S. M. Wang, L. Liu, W. L. Chen, E. B. Wang and Z. M. Su, *Dalton Trans.*, 2013, **42**, 2961.

11 D. L. Long, E. Burkholder and L. Cronin, *Chem. Soc. Rev.*, 2007, **36**, 105.

12 S. Liu, D. G. Kurth, H. Möhwald and D. Volkmer, *Adv. Mater.*, 2002, **14**, 225.

13 (*a*) X. Lopez, J. J. Carbo, C. Bo and J. M. Poblet, *Chem. Soc. Rev.*, 2012, **41**, 7537; (*b*) W. G. Klemperer, *Inorganic Syntheses*, John Wiley & Sons, Inc., Hoboken, NJ, USA, 2007, ch. 15; (*c*) O. Oms, A. Dolbecq and P. Mialane, *Chem. Soc. Rev.*, 2012, **41**, 7497; (*d*) U. Kortz, A. Müller, J. Slageren, J. Schnack, N. S. Dalal and M. Dressel, *Coord. Chem. Rev.*, 2009, **253**, 2315.

14 (*a*) S. Liu, L. Xu, F. Li, W. Guo, Y. Xing and Z. Sun, *Electrochim. Acta*, 2011, **56**, 8156; (*b*) B. Xu, L. Xu, G. Gao and Y. Jin, *Appl. Surf. Sci.*, 2007, **253**, 3190; (*c*) L. Jin, Y. Fang, P. Hu, Y. Zhai, E. Wang and S. Dong, *Chem. Commun.*, 2012, **48**, 2101; (*d*) L. H. Bi, W. H. Zhou, J. G. Jiang and S. J. Dong, *J. Electrochem. Soc.*, 2008, **624**, 269; (*e*) C. Li, K. P. O'Halloran, H. Ma and S. Shi, *J. Phys. Chem. B*, 2009, **113**, 8043; (*f*) S. Liu and Z. Tang, *Nano Today*, 2010, **5**, 267; (*g*) A. Kuhn and F. C. Anson, *Langmuir*, 1996, **12**, 5481; (*h*) I. Moriguchi and J. H. Fendler, *Chem. Mater.*, 1998, **10**, 2205; (*i*) B. Xu, L. Xu, G. Gao, Y. Yang, W. Guo, S. Liu and Z. Sun, *Electrochim. Acta*, 2009, **54**, 2246; (*j*) S. Liu, L. Xu, G. Gao and B. Xu, *Thin Solid Films*, 2009, **517**, 4668.

15 (*a*) S. M. Wang, L. Liu, W. L. Chen, Z. M. Zhang, Z. M. Su and E. B. Wang, *J. Mater. Chem. A*, 2013, **1**, 216; (*b*) S. M. Wang, L. Liu, W. L. Chen and E. B. Wang, *Electrochim. Acta*, 2013, **113**, 240.

16 (*a*) S. P. Harmalker, M. A. Leparulo and M. T. Pope, *J. Am. Chem. Soc.*, 1983, **105**, 4286; (*b*) M. Abbessi, R. Contant, R. Thouvenot and G. Hervé, *Inorg. Chem.*, 1991, **30**, 1695.

17 (*a*) H. Zheng, J. Z. Ou, M. S. Strano, R. B. Kaner, A. Mitchell and K. Kalantar-zadeh, *Adv. Funct. Mater.*, 2011, **21**, 2175; (*b*) C. G. Granqvist, *Thin Solid Films*, 2014, **564**, 1.

18 L. Li, Q. Y. Wu, Y. H. Guo and C. W. Hu, *Microporous Mesoporous Mater.*, 2005, **87**, 1.

19 (*a*) C. S. Hsu, C. K. Lin, C. C. Chan, C. C. Chang and C. Y. Tsay, *Thin Solid Films*, 2006, **494**, 228; (*b*) H. Huang, J. Tian, W. K. Zhang, Y. P. Gan, X. Y. Tao, X. H. Xia and J. P. Tu, *Electrochim. Acta*, 2011, **56**, 4281; (*c*) B. Baloukas, J. M. Lamarre and L. Martinu, *Sol. Energy Mater. Sol. Cells*, 2011, **95**, 807.

20 (*a*) S. S. Kalagi, S. S. Mali, D. S. Dalavi, A. I. Inamdar, H. Im and P. S. Patil, *Synth. Met.*, 2011, **161**, 1105; (*b*) S. S. Kalagi, S. S. Mali, D. S. Dalavi, A. I. Inamdar, H. Im and P. S. Patil, *Electrochim. Acta*, 2012, **85**, 501.

21 R. Contant, W. G. Klemperer and O. Yaghi, *Inorganic Syntheses*, John Wiley & Sons, Inc., Hoboken, NJ, USA, 2007, ch. 18.

22 Z. Xie, L. Gao, B. Liang, X. Wang, G. Chen, Z. Liu, J. Chao, D. Chen and G. Shen, *J. Mater. Chem.*, 2012, **22**, 19904.

